**Title**
Splicing Defects of the Profilin Gene Alter Actin Dynamics in an S. pombe SMN Mutant

**Authors**
Antoine, Marie
Patrick, Kristin L
Soret, Johann
et al.
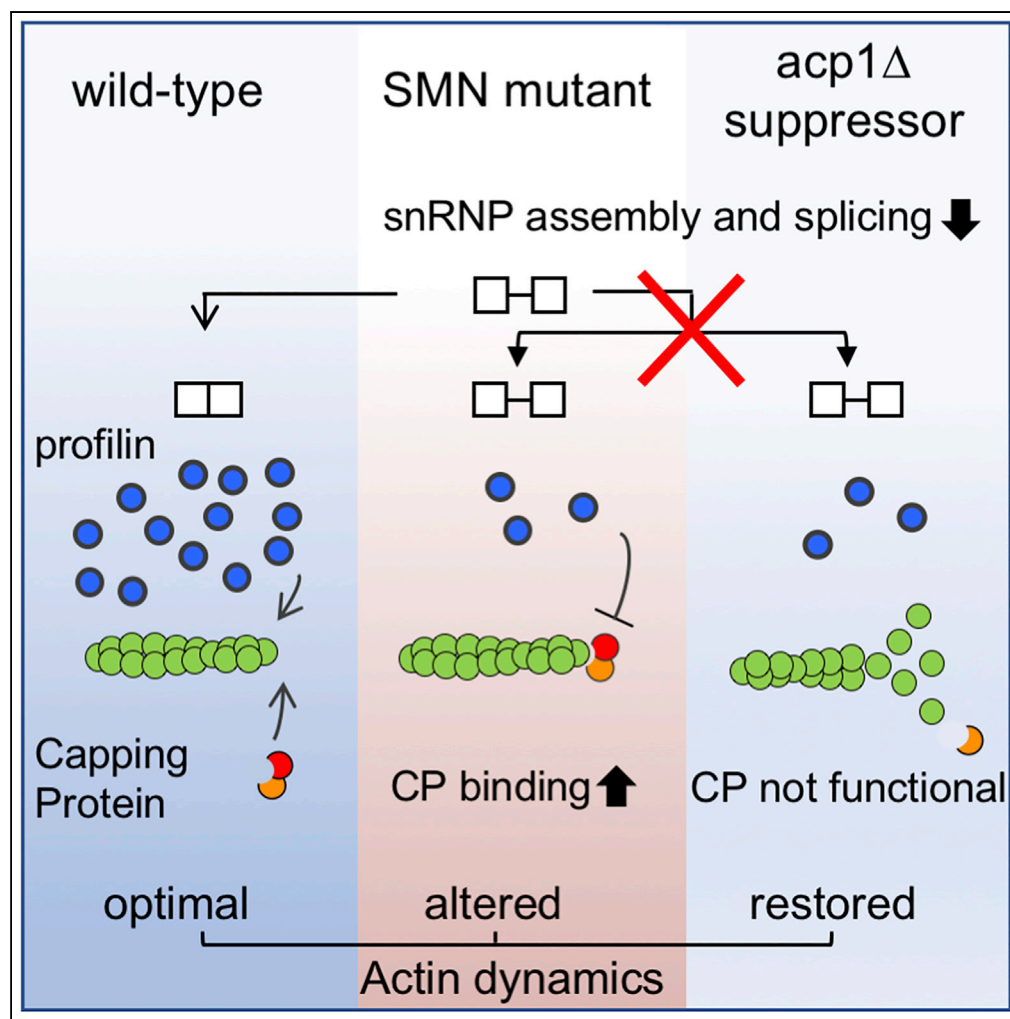
Peer reviewed

## Article

# Splicing Defects of the Profilin Gene Alter Actin Dynamics in an *S. pombe* SMN Mutant

Marie Antoine,
Kristin L. Patrick,
Johann Soret, ...,
Christine Guthrie,
Yannick Gachet,
Rémy Bordonné

remy.bordonne@igmm.cnrs.fr

**HIGHLIGHTS**

Splicing defects in the profilin gene in an *S. pombe* SMN mutant

SMN mutant contains excessively polymerized actin

Altered actin dynamics in the SMN mutant hinders endocytosis and cytokinesis

Deletion of the *acp1* subunit restores actin dynamics in the SMN mutant

## Article

# Splicing Defects of the Profilin Gene Alter Actin Dynamics in an *S. pombe* SMN Mutant

Marie Antoine,[1] Kristin L. Patrick,[2] Johann Soret,[1] Pauline Duc,[1] Florence Rage,[1] Rebecca Cacciottolo,[3] Kelly E. Nissen,[2] Ruben J. Cauchi,[3] Nevan J. Krogan,[2] Christine Guthrie,[2] Yannick Gachet,[4] and Rémy Bordonné[1,5,*]

## SUMMARY

**Spinal muscular atrophy (SMA) is a devastating motor neuron disorder caused by mutations in the *survival motor neuron* (SMN) gene. It remains unclear how SMN deficiency leads to the loss of motor neurons. By screening *Schizosaccharomyces pombe*, we found that the growth defect of an SMN mutant can be alleviated by deletion of the actin-capping protein subunit gene *acp1⁺*. We show that SMN mutated cells have splicing defects in the profilin gene, which thus directly hinder actin cytoskeleton homeostasis including endocytosis and cytokinesis. We conclude that deletion of *acp1⁺* in an SMN mutant background compensates for actin cytoskeleton alterations by restoring redistribution of actin monomers between different types of cellular actin networks. Our data reveal a direct correlation between an impaired function of SMN in snRNP assembly and defects in actin dynamics. They also point to important common features in the pathogenic mechanism of SMA and ALS.**

## INTRODUCTION

Spinal muscular atrophy (SMA) is a common recessive genetic disease and is the leading genetic cause of infant mortality. For 98% of patients, SMA is caused by deletions or mutations in the *survival motor neuron* gene 1 (*SMN1*) (Lefebvre et al., 1995; Lorson et al., 1999). The SMN protein is ubiquitously expressed and interacts with a large number of factors, indicating its involvement in multiple biological pathways.

The best-characterized function of the SMN complex is its role in the biogenesis of spliceosomal small nuclear ribonucleoprotein (snRNP) particles, which are major constituents of the spliceosome, the nuclear pre-mRNAs processing machinery (Liu et al., 1997; Fischer et al., 1997; Pellizzoni et al., 2002; Battle et al., 2006; Chari et al., 2009). Several studies have reported that SMN deficiency alters the stoichiometry of snRNPs in SMN-deficient mouse tissues and causes widespread and tissue-specific pre-mRNA splicing defects in SMA mouse models (Gabanella et al., 2007; Zhang et al., 2008; Baumer et al., 2009). There is also evidence that SMN deficiency gives rise to differential defects and alterations in the splicing of various genes (Boulisfane et al., 2011; Lotti et al., 2012; Doktor et al., 2017). These results support the view that SMA might arise from the inefficient splicing of pre-mRNAs coding for proteins required for motor neurons function and/or survival. However, a non-splicing role is also possible, as axons contain SMN complexes lacking Sm proteins but containing other RNA-binding proteins, suggesting a function for SMN in the assembly of ribonucleoproteins involved in the regulation of mRNA transport, stability, and/or local translation (Burghes and Beattie, 2009; Rossoll and Bassell, 2009; Fallini et al., 2012).

SMN also interacts with proteins associated with cytoskeletal dynamics (Bowerman et al., 2009; Fallini et al., 2012). Integrity of the cytoskeleton is essential for correct function of the synaptic terminal as well as for the axons, and several reports indicate that cytoskeletal dynamics might be impaired in SMA. Indeed, SMN was shown to interact and to co-localize in motor neurons with the small actin-binding proteins profilin I and II, and SMN knockdown induced a stronger interaction between profilin-2 and its upstream kinase ROCK (Giesemann et al., 1999; Bowerman et al., 2007, 2009). Involvement of the actin cytoskeleton in SMA is also based on studies showing that the actin-bundling protein Plastin 3 acts as a protective modifier of SMA in humans (Oprea et al., 2008). Accordingly, *PLS3* overexpression rescues axon outgrowth defects in SMN-deficient zebrafish embryos, in cultured motor neurons, and in mouse models of SMA (Oprea et al., 2008; Hao le et al., 2012; Ackermann et al., 2013; Kaifer et al., 2017). SMN deficiency resulted also in impaired endocytosis in various models of SMA including human, mice, zebrafish, C. elegans, or Drosophila (Dimitriadi et al., 2016; Hosseinbarkooie et al., 2016; Riessland et al., 2017; Janzen et al.,

[1]Institut de Génétique Moléculaire de Montpellier, University of Montpellier, CNRS, Montpellier, France

[2]University of California, San Francisco, CA 94143, USA

[3]Department of Physiology and Biochemistry, University of Malta, Msida, Malta

[4]Centre de Biologie Intégrative, University of Toulouse, CNRS, Toulouse, France

[5]Lead Contact

*Correspondence: remy.bordonne@igmm.cnrs.fr

https://doi.org/10.1016/j.isci.2019.100809

2018). Importantly, endocytosis defects can also be rescued by genetic modifiers such as *PLS3* (Hosseini-barkooie et al., 2016), *NCALD* (Riessland et al., 2017), and *CHP1* (Janzen et al., 2018).

As there is no SMN homolog in the budding yeast *Saccharomyces cerevisiae*, a detailed analysis of the SMN functions has never been possible using genetic and biochemical approaches in this model system. In contrast, the fission yeast *Schizosaccharomyces pombe* contains an SMN gene, which is essential for growth. In this work, we used a genetic approach to find genes able to modulate growth of fission yeast cells carrying a hypomorphic temperature-degron SMN (*tdSMN*) mutant, which has differential snRNP assembly and splicing defects (Campion et al., 2010). We report that deletion of the *acp1*+ gene encoding a subunit of the heterodimeric actin-capping protein has a protective effect on this *tdSMN* mutant. We found also that *tdSMN* cells contain lower levels of profilin and have excessively polymerized and stable actin networks leading to delays in endocytosis, cytokinesis, and cellular growth. Our work provides a framework for understanding how actin dynamics might become altered in SMN-deficient cells.

## RESULTS

### The acp1+ Gene Is a Protective Modifier for SMN-deficient *S. pombe* Cells

To characterize biological pathways connected to SMN, we focused on a hypomorphic fission yeast *tdSMN* mutant displaying a growth defect even at the permissive temperature (Campion et al., 2010). We took an Epistatic MiniArray Profiles (E-MAP) approach (Collins et al., 2010) to screen for deletion strains that either enhance or suppress the tdSMN growth defect. As shown in Table S1, we identified 10 hits with significant scores, which include four suppressors and six enhancers. Remarkably, the vast majority of the encoded proteins have human homologs (Table S1). As expected and based on known links between splicing, chromatin structure, and transcription (Naftelberg et al., 2015), several identified genes have functions in chromatin remodeling, transcription, protein transport, and dephosphorylation. Further validation of the E-MAP screen was provided by identification of the deletion of the fission yeast *icln*+ gene, which encodes a subunit of the PRMT5-complex known to act with the SMN complex in early steps of snRNP biogenesis (Meister et al., 2001; Chari et al., 2008; Barbarossa et al., 2014), as an enhancer of tdSMN growth defect.

To decipher the molecular bases of the protective effects of modifier genes and due to potential links between deregulation of actin dynamics and SMA pathogenesis (Oprea et al., 2008; Bowerman et al., 2009), we focused on the protective/modifier gene *acp1*+ (actin-capping protein of muscle Z-line subunit alpha 1, *CAPZA1* in human), which together with *acp2*+, encodes the heterodimeric actin-capping protein (CP) binding to the fast growing barbed ends of actin filaments. Neither *acp1*+ nor *acp2*+ are required for cell viability, and *S. pombe* cells lacking either capping protein subunits have normal morphology at 25°C (Nakano et al., 2001; Kovar et al., 2005). Throughout this work, we examined the effects of *tdSMN* and *acp1Δ* on cell growth, protein levels, and actin assembly at the permissive temperature (25°C) because tdSMN cells already display snRNP assembly, splicing, and growth defects at 25°C (Campion et al., 2010). The suppressive phenotype of *acp1Δ* was confirmed by a growth assay using serial dilutions of wild-type, *tdSMN,* and *tdSMN acp1Δ* strains (Figure S1A), which showed that the double mutant is slightly healthier than the single *tdSMN* strain. Growth curves also showed a slight improvement in growth upon deletion of *acp1*+ in the *tdSMN* background (Figure S1B).

### tdSMN Cells Contain Higher Levels of Filamentous Actin

To characterize the molecular basis explaining the protective effect of *acp1*+ deletion on the *tdSMN* mutant, we first characterized the filamentous/globular (F/G)-actin ratio in wild-type, *tdSMN*, and *tdSMN acp1Δ* strains. As shown in Figure 1A, when actin is prepared using NaOH/TCA treated extracts, the total amount of actin is similar in all three strains. However, when actin is prepared by differential centrifugation following the protocol of the cytoskeleton *in vivo* F/G-actin assay kit, we found that monomeric G-actin is barely detectable in all strains, whereas F-actin is easily detected and migrates similarly to control rabbit skeletal muscle actin as a 42 kDa protein (Figure 1A). Interestingly, quantification of the blot showed that F-actin is found at lower levels in the wild-type and *tdSMN acp1Δ* cells compared with *tdSMN* cells (Figures 1B and S2).

To confirm levels of F-actin in the strains, quantitative fluorescence microscopy was performed on fixed cells stained with Alexa Fluor 488 phalloidin, which is known to bind tightly and selectively to F-actin polymers. Stacks (z series) of images were acquired at high (63×) magnification, and one section was used to calculate the background-corrected total cell fluorescence (CTCF) from n > 200 cells using ImageJ. Representative images of phalloidin staining are shown in Figures 1C and 1D as well as in Figure S3 for the strains
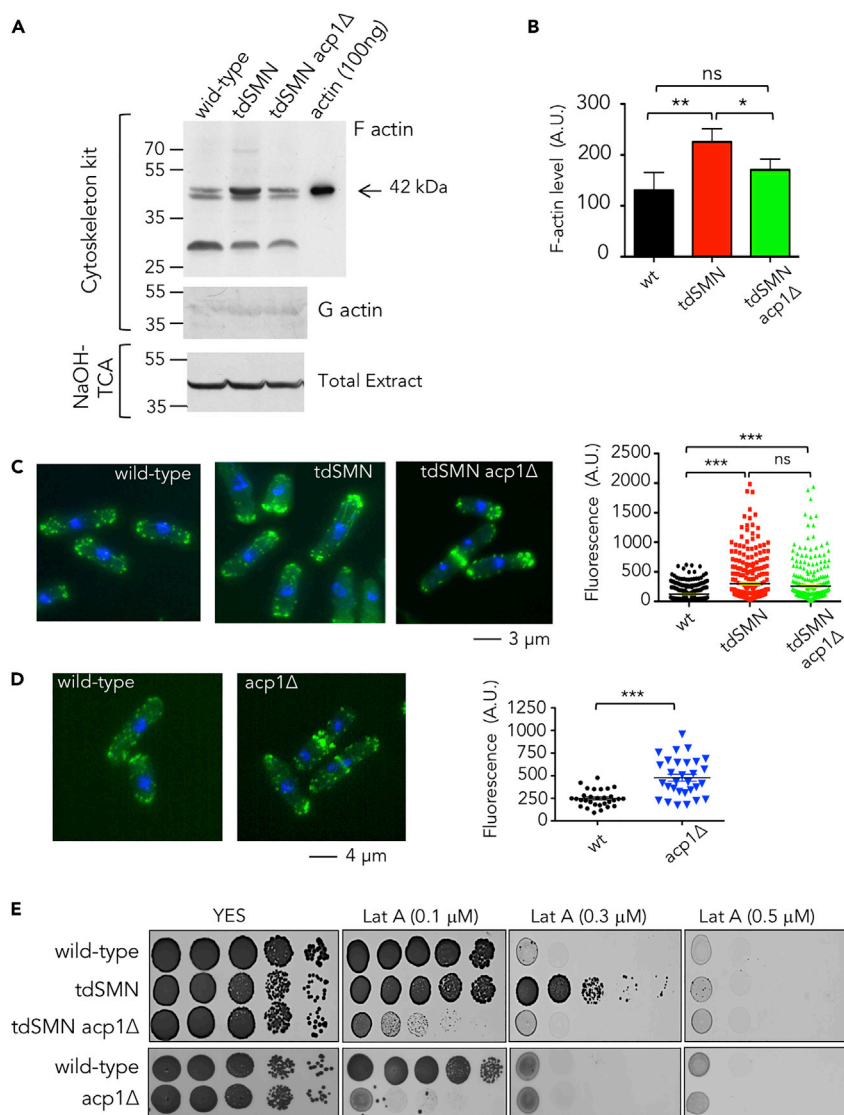
**Figure 1. Increased Levels of Filamentous Actin in *S. pombe* SMN-deficient Cells**

(A) Whole-cell extract and F/G-actin fractions were prepared as described in Experimental Procedures, and equal amounts of fractions for each strain were loaded onto SDS-PAGE gels. Immunoblot was done using the AAN01 actin antibody. Representative data from three independent experiments are shown. A lane containing 100 ng of rabbit skeletal muscle actin was included as control.

(B) Changes in the levels of F-actin observed on blots were quantified using ImageJ. Data are from three independent experiments. Data are presented as mean ± SEM for each category. (**) $p < 0.01$, (*) $p < 0.05$, (ns) non-significant, Tukey's multiple comparison test.

(C) Actin distribution in wild-type, *tdSMN,* and *tdSMN acp1Δ* suppressor cells. The cells were grown at 25°C, fixed with paraformaldehyde and stained for actin with Alexa Fluor 488 phalloidin. DNA was stained with DAPI (blue). Fluorescence was quantified using ImageJ from n > 200 cells for each strain with three trials per genotype. Images were acquired using identical parameters. Data are presented as mean ± SEM for each category. (***) $p < 0.001$, (ns) non-significant, Tukey's multiple comparison test.

(D) Actin distribution was examined in wild-type and *acp1Δ* cells in conditions similar to those described in 1C. Quantification was performed using ImageJ from n = 30 cells with three trials per genotype. (***) $p < 0.001$, two-sided unpaired Student *t* tests.

(E) Latrunculin A sensitivity of strains. Cells were grown in YES media, and serial dilutions were spotted on YES plates containing no or the indicated concentrations of latrunculin A (LatA).

that were grown exponentially under similar conditions. Quantification of the fluorescence intensity showed increased fluorescence in *tdSMN*, *tdSMN acp1Δ*, and *acp1Δ* cells compared with wild type (Figures 1C and 1D), indicating increased levels of F-actin.

We reasoned that higher levels of F-actin in the *tdSMN* mutant could have an impact on actin dynamics. To test this, we monitored the sensitivity of the strains to latrunculin A (LatA), which is a potent inhibitor of F-actin polymerization and has been shown to cause disruption of the actin cytoskeleton (Fujiwara et al., 2018). As shown in Figure 1E, all strains grew on rich media and were sensitive to 0.5 μM LatA. However, on plates containing lower amounts of LatA (0.1 μM), wild-type and *tdSMN* cells were resistant, whereas *tdSMN acp1Δ* and *acp1Δ* cells were hypersensitive. Remarkably, *tdSMN* cells were found to be considerably resistant to 0.3 μM LatA, whereas growth of wild-type, *tdSMN acp1Δ*, and *acp1Δ* cells was inhibited. Altogether, these experiments demonstrate that actin dynamics is altered in *tdSMN* cells and that the *tdSMN* mutant contains excessively polymerized actin compared with wild-type and suppressor cells.

### Analysis of Actin Distribution In Vivo

To investigate actin dynamics in live cells, we constructed strains carrying a *Pact1*-LifeAct-GFP reporter, which allows visualization of the actin cytoskeleton in living cells (Huang et al., 2012). Cells expressing this reporter resemble wild-type cells in morphology, growth rate, and cell division (Huang et al., 2012), indicating that any effects of the reporter on actin dynamics are only subtle (Courtemanche et al., 2016). Expression levels of the LifeAct-GFP reporter were similar in wild-type, *tdSMN*, *tdSMN acp1Δ* suppressor, and *acp1Δ* cells (Figure S4), and all four strains contained the three F-actin structures present in *S. pombe*: endocytic actin patches, cables, and contractile actin rings (Figure 2A). There were clear similarities in the distribution of F-actin in wild-type, *tdSMN acp1Δ*, and *acp1Δ* cells, with all three strains having more bipolar actin and fewer cells with contractile actin rings (Figure 2B). In contrast, the actin patches in *tdSMN* cells often had a monopolar distribution, and the number of *tdSMN* cells containing bipolar actin decreased two-fold. There were also more *tdSMN* cells with actin localized at the contractile actin ring compared with wild-type, suppressor, and *acp1Δ* cells (Figure 2B). As shown in Figure 2C, wild-type and *acp1Δ* monopolar cells had a homogeneous size around 8 μm, whereas *tdSMN* cells were more heterogeneous with elongated cells reaching 15 μm or more, and the sizes of *tdSMN acp1Δ* suppressor cells were more similar to wild-type cells and *acp1Δ* cells. Of the cells with actin localized at the cytokinetic ring, *tdSMN* cells were twice as long compared with wild type, whereas the size of the suppressor cells is between that of wild-type and *tdSMN* cells (Figures 2C and S5). Altogether, these results indicate that *tdSMN* cells have defective actin localization and delayed cytokinesis, which can be partially restored by deletion of the *acp1+* gene.

### tdSMN Cells Display Splicing Defects in the Profilin Gene

Actomyosin ring formation is a highly complex and dynamic process requiring actin remodeling and de novo actin assembly at the division site (Pollard, 2016; Suarez and Kovar, 2016). This actin remodeling is orchestrated by actin-binding proteins including profilin (*cdc3+*), cofilin (*adf1+*), and coronin (*crn1+*). Given that the *S. pombe* genes coding for these regulators contain introns and due to the snRNP assembly and splicing defects observed in the hypomorphic *tdSMN* mutant (Campion et al., 2010), we wondered whether genes coding for these actin-binding proteins might be mis-spliced. Splicing of those three genes were thus analyzed by RT-PCR and as shown in Figure 3A, strong splicing defects can be observed for profilin with clear accumulation of pre-messenger RNAs and a decrease in the level of mature messenger (mRNA) both in the *tdSMN* mutant and *tdSMN acp1Δ* suppressor cells but not in *acp1Δ* cells (Figure S4C). In contrast, no significant splicing defects could be found for cofilin and coronin genes (Figures 3B and 3C, respectively). The decrease in the level of mature profilin mRNA leads to about 80% decrease in the level of profilin protein in *tdSMN* and *tdSMN acp1Δ* cells as measured by Western blot analysis using antibodies directed against *S. pombe* profilin (Figures 3D and 3E).

### Increased Crn1-GFP Fluorescence and Lifetime of Endocytic Patches in tdSMN acp1Δ Suppressor Cells

As mentioned above, profilin, cofilin, and coronin are important molecules for actin-filament remodeling and disassembly. In order to investigate localization of these proteins, we tried to construct tagged versions of the genes by inserting epitopes using homologous recombination. We were unable to obtain tagged genes for profilin and cofilin, and this is due to the fact that the tagged fusion genes are not functional (Wittenmayer et al., 2000; Okreglak and Drubin, 2007). However, we obtained a strain carrying a coronin-GFP fusion gene expressed from its endogenous promoter. As shown by Western blot using anti-GFP antibodies, expression of the fusion protein is similar in wild-type, *tdSMN*, *tdSMN acp1Δ* suppressor,
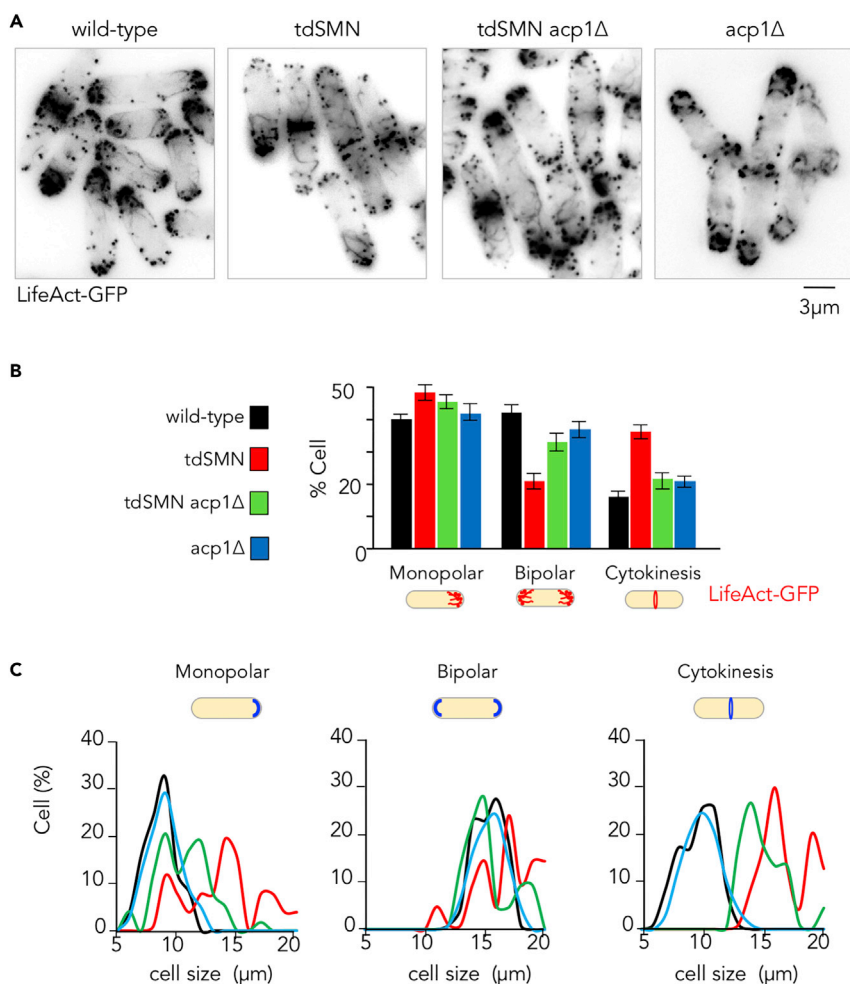
**Figure 2. Cytokinesis Defect of *tdSMN* Mutant Cells**

(A) Comparison of LifeAct-GFP-labeled F-actin structures in wild-type, *tdSMN*, *tdSMN acp1Δ* suppressor, and *acp1Δ* cells. Fluorescence micrographs show that the *S. pombe* actin networks are observed in all four strains. The bar represents 3 μm.

(B) Quantification of (A) showing the percentage of cells with corresponding actin distribution for each indicated strain. Monopolar, actin localized at one end; bipolar, actin at both ends; cytokinesis, actin localized at the cytokinetic ring. Data are represented as the mean from three separate experiments (n = 100) with error bars showing the SD.

(C) Quantification of (A) showing the percentage of cells with corresponding cell sizes (in μm) for cells having actin localized as monopolar, bipolar, or at the cytokinetic ring. Results are from three independent measurements (n = 100). Quantification data are also shown as histograms in Figure S5.

and *acp1Δ* strains (Figure S6). It has been previously reported that Crn1-GFP localizes in patches that are coincident with actin (Sirotkin et al., 2010). Accordingly, Crn1-GFP fluorescence can be observed as patches at the cell tips as well as at the cell division sites in all three strains (Figures 3F and S7). We quantified coronin fluorescence in live cells as a measure of actin accumulation in endocytic patches, and we found that levels of Crn1-GFP are increased in *tdSMN acp1Δ* suppressor and in *acp1Δ* cells (Figure 3G, panel a). Moreover, although identical in wild-type and *tdSMN* cells, the lifetime of patches is also increased in *tdSMN acp1Δ* and *acp1Δ* cells (Figure 3G, panel b). Consistent with studies showing that deletion of *acp1+* increases the peak amount of actin in endocytic patches (Berro and Pollard, 2014), our results indicate that endocytic patches in *tdSMN acp1Δ* suppressor and *acp1Δ* cells might contain higher levels of coronin and actin compared with wild-type and *tdSMN* cells.

## Deletion of acp1+ in the tdSMN Mutant Rescues Partially the Endocytic Process

Because defects in actin dynamics result in perturbations of endocytosis (Gachet and Hyams, 2005), we measured endocytosis using an internalization assay with FM4-64, an amphiphilic fluorescent dye entering cells through
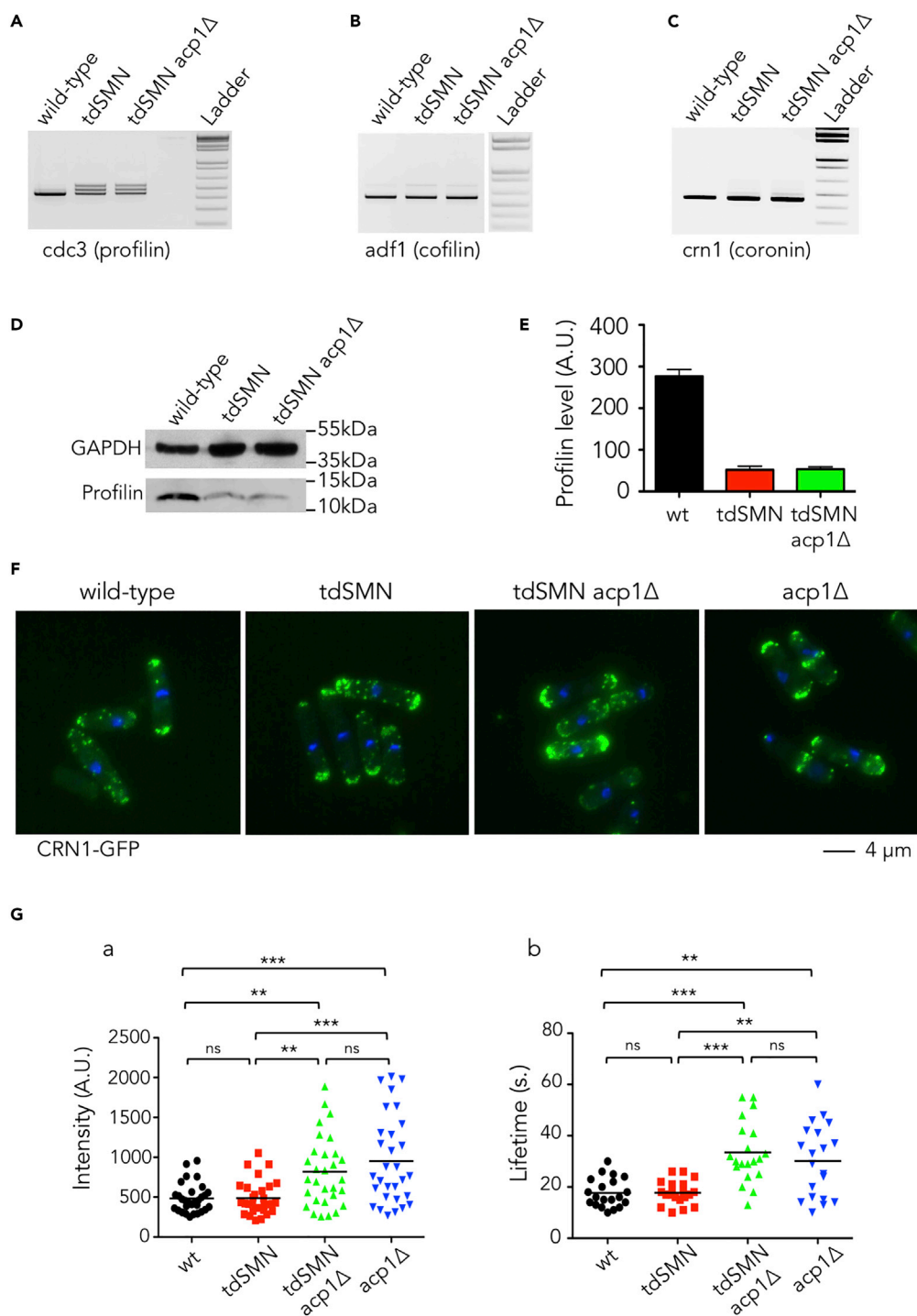
**Figure 3. Fission Yeast SMN-deficient Cells Display Splicing Defects in the Profilin Gene**

(A–C) RT-PCR analyses were performed on total RNA isolated from the wild-type, *tdSMN* mutant, and *tdSMN acp1Δ* suppressor grown at 25°C. The PCR products were separated on a 1.5% agarose gel and visualized by ethidium bromide staining. Tests were performed for introns located in the *S. pombe cdc3+* gene coding for profilin (A), the *adf1+* gene coding for cofilin (B), and the *crn1+* gene coding for coronin (C). The marker corresponds to the invitrogen 1Kb Plus DNA ladder.

(D) Western blot of extracts prepared from the indicated strains using antibodies directed against *S. pombe* profilin. For loading control, GAPDH levels were determined.

**Figure 3. *Continued***

(E) Quantification of (D) with three trials, with error bars showing the SD.

(F) Live-cell GFP images of Crn1-GFP fusion in wild-type, *tdSMN* mutant, *tdSMN acp1Δ* suppressor, and *acp1Δ* cells. DNA was stained with DAPI (blue). See Figure S7 for representative images.

(G) Quantification of intensity (a) (n = 30) and lifetime (b) (n = 20) of endocytic Crn1-GFP patches. Data are presented as dot plots with mean. ns (non-significant), *** (p < 0.001), and ** (p < 0.01) represent statistical significance as determined by ANOVA with Tukey's post-hoc test.

endocytosis (Vida and Emr, 1995). To examine the transport of FM4-64, cells were first incubated with the dye on ice and then chased at 25°C for various times. As shown in Figures 4A and 4B, the dye is transported efficiently into wild-type and *acp1Δ* cells. It is also incorporated in the suppressor cells, whereas in *tdSMN* cells, labeling is highly decreased even after 30 min. Quantification analyses (Figure 4C) confirm that FM4-64 was internalized more slowly in *tdSMN* cells, suggesting that endocytosis is altered in the *tdSMN* hypomorphic mutant. They show also that deletion of *acp1⁺* rescues partly the endocytic process in the *tdSMN acp1Δ* suppressor cells.

## DISCUSSION

Yeast models have been proven to be relevant research tools to study biological pathways and to identify components and mechanisms of many essential cellular processes. They have also been used for identifying the functions of genes related to human diseases, including neurodegenerative diseases (for review, see Fruhmann et al., 2017). In this work, using *S. pombe*, we demonstrate a clear correlation between an impaired function of SMN in snRNP assembly and defects in actin dynamics. We show that SMN deficiency gives rise to splicing defects in the profilin gene leading to decreased cellular levels of profilin. No interaction could be detected between *S. pombe* SMN and profilin by two-hybrid assays (Figure S8), indicating that the observed splicing defects are responsible for the alteration of actin dynamics in the *tdSMN* mutant. Indeed, profilins constitute a family of small monomeric G-actin-binding proteins that are structurally highly conserved and essential for the regulation of filamentous F-actin networks (Jockusch et al., 2007). In both mammalian and yeast cells, overproduction of profilin enhances linear actin arrays and inhibits
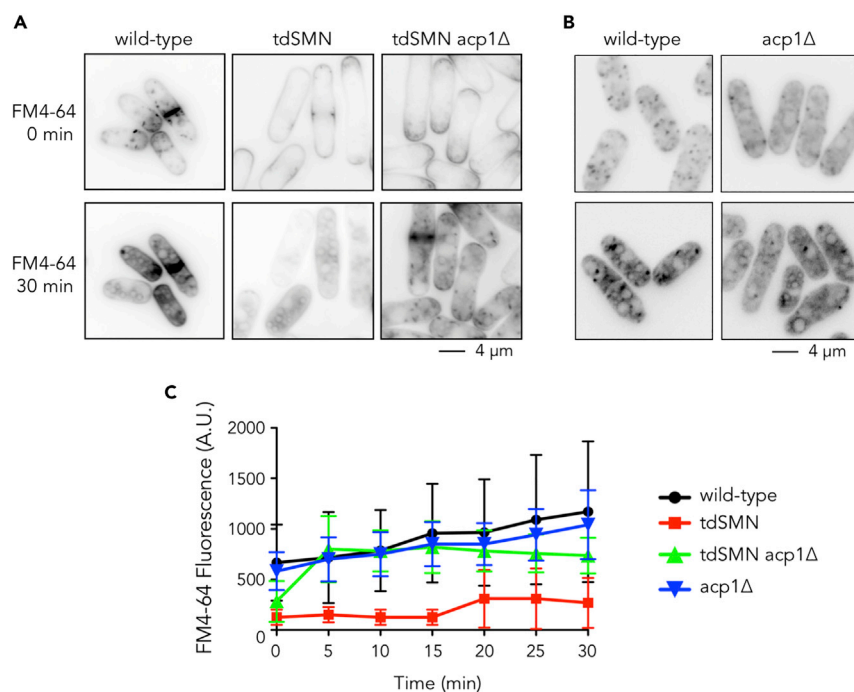


**Figure 4. Fission Yeast SMN-deficient Cells Display an Endocytosis Defect**

(A and B) Analysis of endocytosis was performed for the indicated strains using the lipophilic dye, FM4-64. After incubation with FM4-64 on ice for the indicated time, cells were transferred to an imaging chamber, and images were captured in a single focal plan and the light intensity recorded for 20 cells at each time point. Representative images of cells are shown. Scale bars represent 4 μm.

(C) Quantification of (A) and (B). Data are represented as the mean ± SEM from three separate experiments (n = 20).
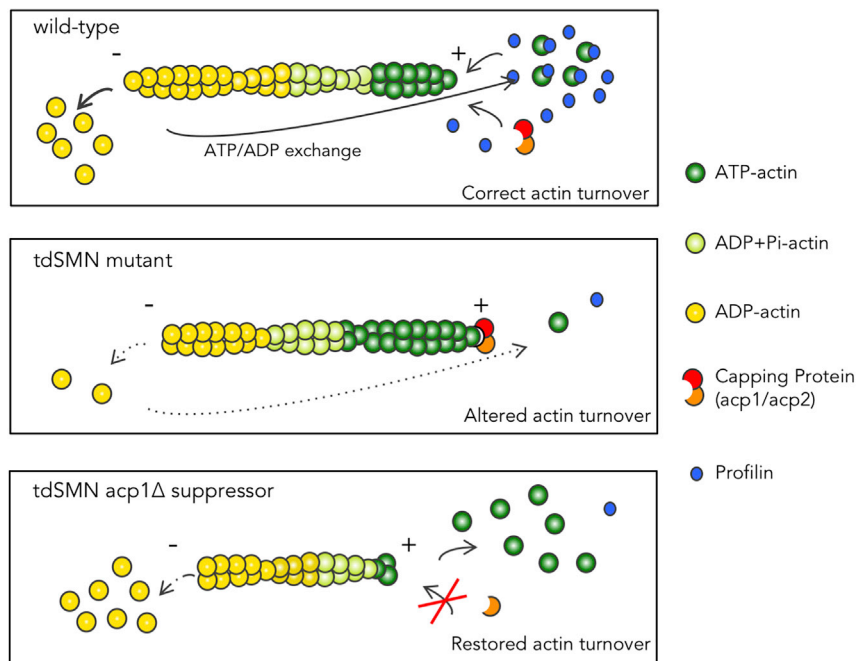
**Figure 5. Model of Actin Dynamics in *S. pombe* Wild-Type, *tdSMN* Mutant, and *tdSMN acp1Δ* Suppressor Cells**

Upper panel: correct actin turnover is achieved in wild-type cells because profilin can compete with the functional capping protein, for binding to barbed ends of actin filaments. Middle panel: in the *tdSMN* mutant, defective splicing downregulates profilin, which perturbs actin turnover by allowing excessive binding of capping protein. Lower panel: deletion of the acp1 subunit of the capping protein in the *tdSMN* mutant removes functional capping protein and thus restores actin dynamics by allowing depolymerisation of actin from barbed ends. This generates increased redistribution of actin monomer to the different actin networks. Pointed (−) and barbed (+) ends are indicated. See also Discussion for details.

short-branched actin networks, whereas lower level of profilin favors such branched actin patches (Burke et al., 2014; Suarez et al., 2015; Rotty et al., 2015). It is also known that modifying profilin levels alters specific F-actin networks and leads to defects in cytokinesis in various cells including fission yeast, worms, and mice (Balasubramanian et al., 1994; Severson et al., 2002; Witke et al., 2001). Our results are thoroughly consistent with profilin being required for proper distribution of actin to different homeostatic F-actin networks (Suarez and Kovar, 2016; Pollard, 2016; Carlier and Shekhar, 2017).

As splicing of profilin is not rescued by deletion of $acp1^+$, the $acp1\Delta$ modifier/protective effect is likely downstream. Accordingly, the heterodimeric capping protein binds to free F-actin barbed-ends with high affinity (Winkelman et al., 2014; Shekhar et al., 2015) and competes also with other barbed-ends regulators such as formins (Kovar et al., 2005) or Aip1 (Berro and Pollard, 2014). It is also known that binding of profilin to barbed-ends enhances the dissociation of actin from barbed ends and thus destabilizes the actin filaments (Jégou et al., 2011; Pernier et al., 2016). Our results are consistent with these observations and support the model for actin dynamics depicted in Figure 5. In this model, due to decreased levels of profilin in the *tdSMN* mutant, profilin is unable to compete with proteins binding to barbed ends including the capping protein, which can therefore bind to excessive numbers of barbed ends, enhancing stabilization of actin filaments. As a consequence, the pool of actin available for the formation of new actin networks is low, and this generates the endocytosis and cytokinesis delays observed in the *tdSMN* mutant. Upon deletion of the $acp1^+$ gene in *tdSMN* cells, the capping protein is not functional enabling actin depolymerization from barbed ends. This refills the pool of polymerizable actin restoring actin turnover/distribution to other networks and alleviates partially the *tdSMN* growth defect. The *tdSMN acp1Δ* suppressor exhibits also increased binding of coronin as shown by enhanced fluorescence of actin patches in cells expressing an endogenous Crn1-GFP reporter (Figure 3G). Because it has been reported that coronin cooperates with actin-binding regulators to sever older filaments (Gandhi and Goode, 2008), the suppressive mechanism of $acp1^+$ deletion in the *tdSMN* background could indeed be due to increased availability of actin molecules. Our results are in agreement with the view that profilin orchestrates actin homeostasis and with the
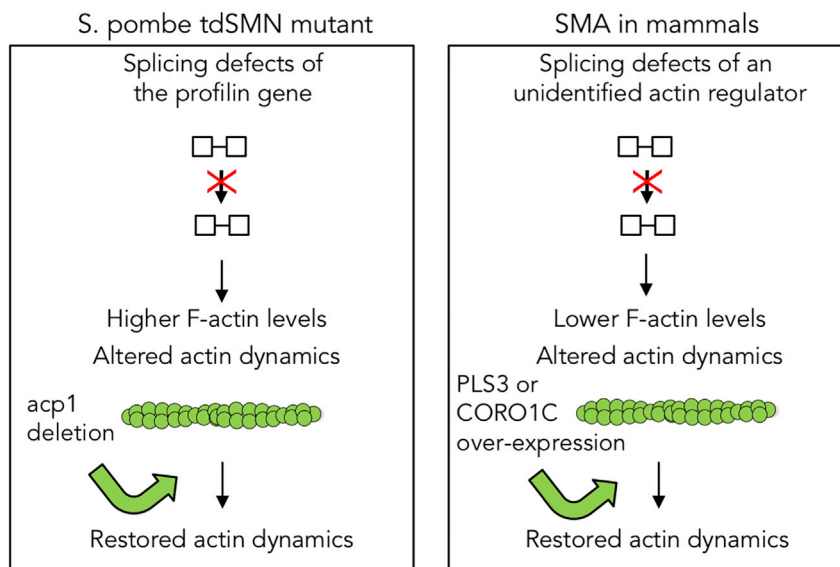
**Figure 6. Schematic Depiction of Events Leading to Alterations and Rescues of Actin Dynamics in SMN-deficient *S. pombe* and Mammalian SMA Models**

In the *tdSMN* mutant, due to splicing defects, profilin levels are decreased, giving rise to higher levels of F-actin and altering actin dynamics. Correct actin dynamics can be restored by deletion of the *acp1⁺* gene. For SMA in mammals, we propose that splicing defects lead to decreased levels of an unidentified actin regulator, and this results in lower levels of F-actin and alterations in actin dynamics, which can be suppressed by overexpression of *PLS3* or *CORO1C* (Hosseinibarkooie et al., 2016; Kaifer et al., 2017).

emerging notion that competition for limited amounts of actin monomers represents an important regulatory mechanism for the organization of actin cytoskeletal networks and for cellular growth (Suarez and Kovar, 2016; Pollard, 2016; Carlier and Shekhar, 2017).

Our work shows also that *tdSMN* cells contain extensively polymerized actin networks, which are more resistant to depolymerization as shown by increased growth on plates containing LatA (Figure 1E). Although F-actin dynamics and localization are also impaired in SMA mouse models (Ackermann et al., 2013; Gabanella et al., 2016), it is interesting to note that levels of F-actin are significantly reduced upon SMN knockdown at the presynaptic site at the NMJ structure as well as in NSC34 and HEK293T cells (Ackermann et al., 2013; Hosseinibarkooie et al., 2016). As depicted in Figure 6, this apparent contradiction in the amounts of F-actin found in the S. pombe *tdSMN* mutant and SMA cells could be explained by the fact that splicing defects of an unidentified actin regulator, different of profilin, might be responsible for the observed alterations in actin dynamics in mammalian models of SMA. According to this view, defective splicing has never been observed for profilin genes in studies aimed to characterize splicing defects in mammalian SMA models (Zhang et al., 2008; Baumer et al., 2009; Lotti et al., 2012).

A stabilized actin network could also explain the observed perturbation of the endocytic pathway in *tdSMN* cells (Figure 4). As already mentioned in the Introduction, defects in endocytosis were also observed when SMN levels were compromised in various SMA models (Dimitriadi et al., 2016; Hosseinibarkooie et al., 2016; Riessland et al., 2017; Janzen et al., 2018). In mice particularly, it has been shown that endocytic defects can be restored by overexpression of Plastin 3 or Coronin 1C, which are F-actin-binding and -bundling proteins. Remarkably, the capping protein was also co-immunoprecipitated from *PLS3*-overexpressing HEK293T cells, indicating that it is part of a unique functional complex (Hosseinibarkooie et al., 2016). It is thus possible that restoration of actin dynamics might also represent the mechanism leading to the rescue of endocytic trafficking observed in SMA mice.

Several studies have also identified mutations in the *PFN1* gene in human familial amyotrophic lateral sclerosis (ALS) patients (Smith et al., 2015). Accordingly, novel mouse models carrying profilin-1 mutations show abnormal F/G-actin ratio in spinal cords and have physical and mental ALS-like phenotypes (Fil et al., 2017). Given that cytoskeletal defects in the brain and spinal cord tissues emerge as one of the

most important causes of motor neuron vulnerability, it is tempting to speculate that SMA could also be caused by splicing alterations in genes playing a role in actin dynamics (Figure 6). In this regard, a recent transcriptomic study has reported a significant downregulation of the axon-guidance pathway in spinal cords of postnatal day 5 SMA mice (Doktor et al., 2017). This is particularly intriguing because formation of axons is dependent on crosstalks between actin filaments and the microtubule cytoskeleton (Blanquie and Bradke, 2018). Future work will be necessary to define precisely the splicing pattern of many attractive candidates including genes coding for the various actin-binding partners, many isoforms being implicated in the assembly of different actin cellular structures.

### Limitations of the Study

Our study shows that splicing defects in the profilin gene occur in the fission yeast *tdSMN* hypomorphic mutant and lead to alterations in actin dynamics. However, given that splicing capabilities are lowered in *tdSMN* cells, it is likely that additional splicing defects take place in other pre-mRNAs, indicating that multiple cellular processes might be affected in the *tdSMN* mutant. Moreover, the direct relevance of this work to SMA disease progression remains to be determined using *in vivo* studies in mammalian systems.

### METHODS

All methods can be found in the accompanying Transparent Methods supplemental file.

### SUPPLEMENTAL INFORMATION

Supplemental Information can be found online at https://doi.org/10.1016/j.isci.2019.100809.

### AUTHOR CONTRIBUTIONS

Investigation, M.A., K.P., R.C., K.N., J.S., F.R., P.D., Y.G., and R.B.; Resources, Ru.C., N.K., C.G., and R.B.; Supervision, R.B.; Writing—Original draft, R.B.; Writing—Review and editing, Ru.C., Y.G., and R.B.; Funding acquisition, R.B.

### DECLARATION OF INTERESTS

The authors declare no competing interests.

### REFERENCES

Ackermann, B., Kröber, S., Torres-Benito, L., Borgmann, A., Peters, M., Hosseinibarkooie, S.M., Tejero, R., Jakubik, M., Schreml, J., Milbradt, J., et al. (2013). Plastin 3 ameliorates spinal muscular atrophy via delayed axon pruning and improves neuromuscular junction functionality. Hum. Mol. Genet. *22*, 1328–1347.

Balasubramanian, M.K., Hirani, B.R., Burke, J.D., and Gould, K.L. (1994). The Schizosaccharomyces pombe cdc3+ gene encodes a profilin essential for cytokinesis. J. Cell Biol. *125*, 1289–1301.

Barbarossa, A., Antoine, E., Neel, H., Gostan, T., Soret, J., and Bordonné, R. (2014).

Characterization and in vivo functional analysis of the *Schizosaccharomyces pombe* ICLN gene. Mol. Cell Biol. *34*, 595–605.

Battle, D.J., Lau, C.K., Wan, L., Deng, H., Lotti, F., and Dreyfuss, G. (2006). The Gemin5 protein of the SMN complex identifies snRNAs. Mol. Cell *23*, 273–279.

Baumer, D., Lee, S., Nicholson, G., Davies, J.L., Parkinson, N.J., Murray, L.M., Gillingwater, T.H., Ansorge, O., Davies, K.E., and Talbot, K. (2009). Alternative splicing events are a late feature of pathology in a mouse model of spinal muscular atrophy. PLoS Genet. *5*, e1000773.

Berro, J., and Pollard, T.D. (2014). Synergies between Aip1p and capping protein subunits (Acp1p and Acp2p) in clathrin-mediated endocytosis and cell polarization in fission yeast. Mol. Biol. Cell *25*, 3515–3527.

Blanquie, O., and Bradke, F. (2018). Cytoskeleton dynamics in axon regeneration. Curr. Opin. Neurobiol. *51*, 60–69.

Boulisfane, N., Choleza, M., Rage, F., Neel, H., Soret, J., and Bordonné, R. (2011). Impaired minor tri-snRNP assembly generates differential splicing defects of U12-type introns in

lymphoblasts derived from a type I SMA patient. Hum. Mol. Genet. 20, 641–648.

Bowerman, M., Shafey, D., and Kothary, R. (2007). Smn depletion alters profilin II expression and leads to upregulation of the RhoA/ROCK pathway and defects in neuronal integrity. J. Mol. Neurosci. 32, 120–131.

Bowerman, M., Anderson, C.L., Beauvais, A., Boyl, P.P., Witke, W., and Kothary, R. (2009). SMN, profilin IIa and plastin 3: a link between the deregulation of actin dynamics and SMA pathogenesis. Mol. Cell Neurosci. 42, 66–74.

Burghes, A.H., and Beattie, C.E. (2009). Spinal muscular atrophy: why do low levels of survival motor neuron protein make motor neurons sick? Nat. Rev. Neurosci. 10, 597–609.

Burke, T.A., Christensen, J.R., Barone, E., Suarez, C., Sirotkin, V., and Kovar, D.R. (2014). Homeostatic actin cytoskeleton networks are regulated by assembly factor competition for monomers. Curr. Biol. 24, 579–585.

Campion, Y., Neel, H., Gostan, T., Soret, J., and Bordonné, R. (2010). Differential splicing defects in fission yeast cells carrying a temperature-degron allele of the Survival of Motor Neuron gene. EMBO J. 29, 1817–1829.

Carlier, M., and Shekhar, S. (2017). Global treadmilling coordinates actin turnover and controls the size of actin networks. Nat. Rev. Mol. Cell Biol. 18, 389–401.

Chari, A., Golas, M.M., Klingenhager, M., Neuenkirchen, N., Sander, B., Englbrecht, C., Sickmann, A., Stark, H., and Fischer, U. (2008). An assembly chaperone collaborates with the SMN complex to generate spliceosomal SnRNPs. Cell 135, 497–509.

Chari, A., Paknia, E., and Fischer, U. (2009). The role of RNP biogenesis in spinal muscular atrophy. Curr. Opin. Cell Biol. 21, 387–393.

Collins, S.R., Roguev, A., and Krogan, N.J. (2010). Quantitative genetic interaction mapping using the E-MAP approach. Methods Enzymol. 470, 205–231.

Courtemanche, N., Pollard, T.D., and Chen, Q. (2016). Avoiding artefacts when counting polymerized actin in live cells with LifeAct fused to fluorescent proteins. Nat. Cell Biol. 18, 676–683.

Dimitriadi, M., Derdowski, A., Kalloo, G., Maginnis, M.S., O'Hern, P., Bliska, B., Sorkaç, A., Nguyen, K.C., Cook, S.J., Poulogiannis, G., et al. (2016). Decreased function of survival motor neuron protein impairs endocytic pathways. Proc. Natl. Acad. Sci. U S A 113, E4377–E4386.

Doktor, T.K., Hua, Y., Andersen, H.S., Brøner, S., Liu, Y.H., Wieckowska, A., Dembic, M., Bruun, G.H., Krainer, A.R., and Andresen, B.S. (2017). RNA-sequencing of a mouse-model of spinal muscular atrophy reveals tissue-wide changes in splicing of U12-dependent introns. Nucleic Acids Res. 45, 395–416.

Fallini, C., Bassell, G.J., and Rossoll, W. (2012). Spinal muscular atrophy: the role of SMN in axonal mRNA regulation. Brain Res. 1462, 81–92.

Fil, D., DeLoach, A., Yadav, S., Alkam, D., MacNicol, M., Singh, A., Compadre, C.M., Goellner, J.J., O'Brien, C.A., Fahmi, T., et al. (2017). Mutant Profilin1 transgenic mice recapitulate cardinal features of motor neuron disease. Hum. Mol. Genet. 26, 686–701.

Fischer, U., Liu, Q., and Dreyfuss, G. (1997). The SMN-SIP1 complex has an essential role in spliceosomal snRNP biogenesis. Cell 90, 1023–1029.

Fruhmann, G., Seynnaeve, D., Zheng, J., Ven, K., Molenberghs, S., Wilms, T., Liu, B., Winderickx, J., and Franssens, V. (2017). Yeast buddies helping to unravel the complexity of neurodegenerative disorders. Mech. Ageing Dev. 161, 288–305.

Fujiwara, I., Zweifel, M.E., Courtemanche, N., and Pollard, T.D. (2018). Latrunculin A accelerates actin filament depolymerization in addition to sequestering actin monomers. Curr. Biol. 28, 3183–3192.

Gabanella, F., Butchbach, M.E.R., Saieva, L., Carissimi, C., Burghes, A.H.M., and Pellizzoni, L. (2007). Ribonucleoprotein assembly defects correlate with spinal muscular atrophy severity and preferentially affect a subset of spliceosomal snRNPs. PLoS One 2, e921.

Gabanella, F., Pisani, C., Borreca, A., Farioli-Vecchioli, S., Ciotti, M.T., Ingegnere, T., Onori, A., Ammassari-Teule, M., Corbi, N., Canu, N., et al. (2016). SMN affects membrane remodelling and anchoring of the protein synthesis machinery. J. Cell Sci. 129, 804–816.

Gachet, Y., and Hyams, J.S. (2005). Endocytosis in fission yeast is spatially associated with the actin cytoskeleton during polarised cell growth and cytokinesis. J. Cell Sci. 118, 4231–4242.

Gandhi, M., and Goode, B.L. (2008). Coronin: the double-edged sword of actin dynamics. Subcell Biochem. 48, 72–87.

Giesemann, T., Rathke-Hartlieb, S., Rothkegel, M., Bartsch, J.W., Buchmeier, S., Jockusch, B.M., and Jockusch, H. (1999). A role for polyproline motifs in the spinal muscular atrophy protein SMN. Profilins bind to and colocalize with smn in nuclear gems. J. Biol. Chem. 274, 37908–37914.

Hao le, T., Wolman, M., Granato, M., and Beattie, C.E. (2012). Survival motor neuron affects plastin 3 protein levels leading to motor defects. J. Neurosci. 32, 5074–5084.

Hosseinibarkooie, S., Peters, M., Torres-Benito, L., Rastetter, R.H., Hupperich, K., Hoffmann, A., Mendoza-Ferreira, N., Kaczmarek, A., Janzen, E., Milbradt, J., et al. (2016). The power of human protective modifiers: PLS3 and CORO1C unravel impaired endocytosis in spinal muscular atrophy and rescue SMA phenotype. Am. J. Hum. Genet. 99, 647–665.

Huang, J., Huang, Y., Yu, H., Subramanian, D., Padmanabhan, A., Thadani, R., Tao, Y., Tang, X., Wedlich-Soldner, R., and Balasubramanian, M.K. (2012). Nonmedially assembled F-actin cables incorporate into the actomyosin ring in fission yeast. J. Cell Biol. 199, 831–847.

Janzen, E., Mendoza-Ferreira, N., Hosseinibarkooie, S., Schneider, S., Hupperich, K., Tschanz, T., Grysko, V., Riessland, M., Hammerschmidt, M., Rigo, F., et al. (2018). CHP1

reduction ameliorates spinal muscular atrophy pathology by restoring calcineurin activity and endocytosis. Brain 141, 2343–2361.

Jégou, A., Niedermayer, T., Orbán, J., Didry, D., Lipowsky, R., Carlier, M.F., and Romet-Lemonne, G. (2011). Individual actin filaments in a microfluidic flow reveal the mechanism of ATP hydrolysis and give insight into the properties of profilin. PLoS Biol. 9, e1001161.

Jockusch, B.M., Murk, K., and Rothkegel, M. (2007). The profile of profilins. Rev. Physiol. Biochem. Pharmacol. 159, 131–149.

Kaifer, K.A., Villalón, E., Osman, E.Y., Glascock, J.J., Arnold, L.L., Cornelison, D.D.W., and Lorson, C.L. (2017). Plastin-3 extends survival and reduces severity in mouse models of spinal muscular atrophy. JCI Insight 2, e89970.

Kovar, D.R., Wu, J.Q., and Pollard, T.D. (2005). Profilin-mediated competition between capping protein and formin Cdc12p during cytokinesis in fission yeast. Mol. Biol. Cell 16, 2313–2324.

Lefebvre, S., Bürglen, L., Reboullet, S., Clermont, O., Burlet, P., Viollet, L., Benichou, B., Cruaud, C., Millasseau, P., and Zeviani, M. (1995). Identification and characterization of a spinal muscular atrophy-determining gene. Cell 80, 155–165.

Liu, Q., Fischer, U., Wang, F., and Dreyfuss, G. (1997). The spinal muscular atrophy disease gene product, SMN, and its associated protein SIP1 are in a complex with spliceosomal snRNP proteins. Cell 90, 1013–1021.

Lorson, C.L., Hahnen, E., Androphy, E.J., and Wirth, B. (1999). A single nucleotide in the SMN gene regulates splicing and is responsible for spinal muscular atrophy. Proc. Natl. Acad. Sci. U S A 96, 6307–6311.

Lotti, F., Imlach, W.L., Saieva, L., Beck, E.S., Hao le, T., Li, D.K., Jiao, W., Mentis, G.Z., Beattie, C.E., McCabe, B.D., and Pellizzoni, L. (2012). An SMN-dependent U12 splicing event essential for motor circuit function. Cell 151, 440–454.

Meister, G., Eggert, C., Buhler, D., Brahms, H., Kambach, C., and Fischer, U. (2001). Methylation of Sm proteins by a complex containing PRMT5 and the putative U snRNP assembly factor pICln. Curr. Biol. 11, 1990–1994.

Naftelberg, S., Schor, I.E., Ast, G., and Kornblihtt, A.R. (2015). Regulation of alternative splicing through coupling with transcription and chromatin structure. Annu. Rev. Biochem. 84, 165–198.

Nakano, K., Satoh, K., Morimatsu, A., Ohnuma, M., and Mabuchi, I. (2001). Interactions among a fimbrin, a capping protein, and an actin-depolymerizing factor in organization of the fission yeast actin cytoskeleton. Mol. Biol. Cell 12, 3515–3526.

Okreglak, V., and Drubin, D.G. (2007). Cofilin recruitment and function during actin-mediated endocytosis dictated by actin nucleotide state. J. Cell Biol. 178, 1251–1264.

Oprea, G.E., Kröber, S., McWhorter, M.L., Rossoll, W., Müller, S., Krawczak, M., Bassell, G.J., Beattie, C.E., and Wirth, B. (2008). Plastin 3 is a protective

modifier of autosomal recessive spinal muscular atrophy. Science 320, 524–527.

Pellizzoni, L., Yong, J., and Dreyfuss, G. (2002). Essential role for the SMN complex in the specificity of snRNP assembly. Science 298, 1775–1779.

Pernier, J., Shekhar, S., Jegou, A., Guichard, B., and Carlier, M.F. (2016). Profilin interaction with actin filament barbed end controls dynamic instability, capping, branching, and motility. Dev. Cell 36, 201–214.

Pollard, T.D. (2016). Actin and actin-binding proteins. Cold Spring Harb Perspect. Biol. 8, a018226.

Riessland, M., Kaczmarek, A., Schneider, S., Swoboda, K.J., Löhr, H., Bradler, C., Grysko, V., Dimitriadi, M., Hosseinibarkooie, S., Torres-Benito, L., et al. (2017). Neurocalcin delta suppression protects against spinal muscular atrophy in humans and across species by restoring impaired endocytosis. Am. J. Hum. Genet. 100, 297–315.

Rossoll, W., and Bassell, G.J. (2009). Spinal muscular atrophy and a model for survival of motor neuron protein function in axonal ribonucleoprotein complexes. Results Probl. Cell Differ. 48, 289–326.

Rotty, J.D., Wu, C., Haynes, E.M., Suarez, C., Winkelman, J.D., Johnson, H.E., Haugh, J.M.,

Kovar, D.R., and Bear, J.E. (2015). Profilin-1 serves as a gatekeeper for actin assembly by arp2/3-dependent and -independent pathways. Dev. Cell 32, 54–67.

Severson, A.F., Baillie, D.L., and Bowerman, B. (2002). A Formin Homology protein and a profilin are required for cytokinesis and Arp2/3-independent assembly of cortical microfilaments in C. elegans. Curr. Biol. 12, 2066–2075.

Shekhar, S., Kerleau, M., Kühn, S., Pernier, J., Romet-Lemonne, G., Jégou, A., and Carlier, M.F. (2015). Formin and capping protein together embrace the actin filament in a ménage à trois. Nat. Commun. 6, 8730.

Sirotkin, V., Berro, J., Macmillan, K., Zhao, L., and Pollard, T.D. (2010). Quantitative analysis of the mechanism of endocytic actin patch assembly and disassembly in fission yeast. Mol. Biol. Cell 21, 2894–2904.

Smith, B.N., Vance, C., Scotter, E.L., Troakes, C., Wong, C.H., Topp, S., Maekawa, S., King, A., Mitchell, J.C., Lund, K., et al. (2015). Novel mutations support a role for Profilin 1 in the pathogenesis of ALS. Neurobiol. Aging 36, 1602.e17–1602.e27.

Suarez, C., Carroll, R.T., Burke, T.A., Christensen, J.R., Bestul, A.J., Sees, J.A., James, M.L., Sirotkin, V., and Kovar, D.R. (2015). Profilin regulates F-actin network homeostasis by favoring formin over arp2/3 complex. Dev. Cell 32, 43–53.

Suarez, C., and Kovar, D.R. (2016). Internetwork competition for monomers governs actin cytoskeleton organization. Nat. Rev. Mol. Cell Biol. 17, 799–810.

Vida, T.A., and Emr, S.D. (1995). A new vital stain for visualizing vacuolar membrane dynamics and endocytosis in yeast. J. Cell Biol. 128, 779–792.

Winkelman, J.D., Bilancia, C.G., Peifer, M., and Kovar, D.R. (2014). Ena/VASP Enabled is a highly processive actin polymerase tailored to self-assemble parallel-bundled F-actin networks with Fascin. Proc. Natl. Acad. Sci. U S A 111, 4121–4126.

Witke, W., Sutherland, J.D., Sharpe, A., Arai, M., and Kwiatkowski, D.J. (2001). Profilin I is essential for cell survival and cell division in early mouse development. Proc. Natl. Acad. Sci. U S A 98, 3832–3836.

Wittenmayer, N., Rothkegel, M., Jockusch, B.M., and Schlüter, K. (2000). Functional characterization of green fluorescent protein-profilin fusion proteins. Eur. J. Biochem. 267, 5247–5256.

Zhang, Z., Lotti, F., Dittmar, K., Younis, I., Wan, L., Kasim, M., and Dreyfuss, G. (2008). SMN deficiency causes tissue-specific perturbations in the repertoire of snRNAs and widespread defects in splicing. Cell 133, 585–600.

**Supplemental Information**

**Splicing Defects of the Profilin Gene**

**Alter Actin Dynamics in an *S. pombe* SMN Mutant**

Marie Antoine, Kristin L. Patrick, Johann Soret, Pauline Duc, Florence Rage, Rebecca Cacciottolo, Kelly E. Nissen, Ruben J. Cauchi, Nevan J. Krogan, Christine Guthrie, Yannick Gachet, and Rémy Bordonné

Table S1-List of genes whose deletion supresses or enhances tdSMN growth defect. Descriptive informations are from the PomBase database. The S-Score reflects measured colonies sizes of the double mutant. Related to Figure 1.

| Effect | Deleted gene | Human homolog | Description/function | S-Score |
|---|---|---|---|---|
| Suppressor | acp1 | CAPZA1 | F-actin capping protein alpha subunit | 5,81 |
| Suppressor | nup97 | NUP93 | nucleoporin | 5,73 |
| Suppressor | pex13 | PEX13 | protein import into peroxisome | 5,49 |
| Suppressor | SPAC9G1.10c | INPP5J | inositol polyphosphate phosphatase | 5,4 |
| | | | | |
| Enhancer | png2 | ING2 | chromatin remodeling | -12,48 |
| Enhancer | snf59 | | chromatin remodeling | -13,36 |
| Enhancer | nem1 | CTDNEP1 | phosphoprotein phosphatase activity | -13,46 |
| Enhancer | rpb9 | POLR21 | subunit RNA polymerase II | -15,08 |
| Enhancer | swd1 | RBBP5 | WD40, chromatin remodeling | -15,6 |
| Enhancer | icln | ICLN1 | chaperone regulating snRNP assembly | -17,9 |

Table S2-List of the main *S. pombe* strains used in this study; related to methods and to Figures 1-3.

| Strain name | Relevant genotype | Source |
|---|---|---|
| SP200 | leu1-32 ura4-D18 ade6-M210 h- | lab stock |
| SP819 | leu1-32 ura4-D18 ade6-M216 h+ | lab stock |
| PEM-2 | leu1-32 ura4-D18 ade6-M210 mat1-m-cyh$^S$ smt10 rp142::cyh$^R$ (SP56Q) h- | Krogan lab - Roguev et al. 2007 |
| tdSMN | tdSMN (kan$^R$) leu1-32 ura4-D18 ade6-M216 h+ | Campion et al. 2010-lab stock |
| acp1Δ | ura4-D18 leu1-32 ade6-M210 SPAC12B10.07::kan$^R$ h- | Bioneer null mutant |
| tdSMN acp1Δ | tdSMN (kan$^R$) SPAC12B10.07::kan$^R$ ura4-D18 leu1-32 ade6-M210 h- | this study |
| SPRB100 | crn1-GFP-hyg$^R$ leu1-32 ura4-D18 ade6-M210 h- | this study |
| SPRB101 | crn1-GFP-hyg$^R$ tdSMN (kan$^R$) leu1-32 ura4-D18 ade6-M210 h- | this study |
| SPRB102 | crn1-GFP-hyg$^R$ tdSMN (kan$^R$) SPAC12B10.07::kan$^R$ ura4-D18 leu1-32 ade6-M210 h- | this study |
| SPRB103 | crn1-GFP-hyg$^R$ SPAC12B10.07::kan$^R$ ura4-D18 leu1-32 ade6-M210 h- | this study |

Table S3- Primer sequences. Related to Figure 3.

| Primer Name | Sequence |
| --- | --- |
| Cdc3Fw | CAAGTTTTCCTATCTCTAAACC |
| Cdc3Rev | GCAGTAATATTGATTGTCATGTC |
| Adf1Fw | GCTATCAGTAAATAAATAATATG |
| Adf1Rev | CTATTGACAAATTAAATATCAACAG |
| Crn1E1F | CTCATTCGATCTTATAAAGG |
| Crn1E5R | GATGATATTGAACAAGACCAAC |
| Crn1upF | CTCATCCGTCCTCCTTCCTATTCCG |
| Crn1downR | CCATATCTTTTCCTACATTTGTAAATATTGAGG |
| nmt1F | GGAATCCTGGCATATCATC |
| nmt1R | ATATGCAGCTTGAATGGGC |
| kanaF | CCTATGGAACTGCCTCGGTGAG |
| kanaR | TAATTTAAGGTTGTACCTACGAC |
| GFP-F | GAGAGACCACATGGTCCTTCTTG |
| GFP-R | CCACTGACAGAAAATTTGTGCC |
| acp1upF | GACGACCTCCGAGGCTATATTTAC |
| acp1downR | CCCTTAAATTACTGGTGACGAGCG |
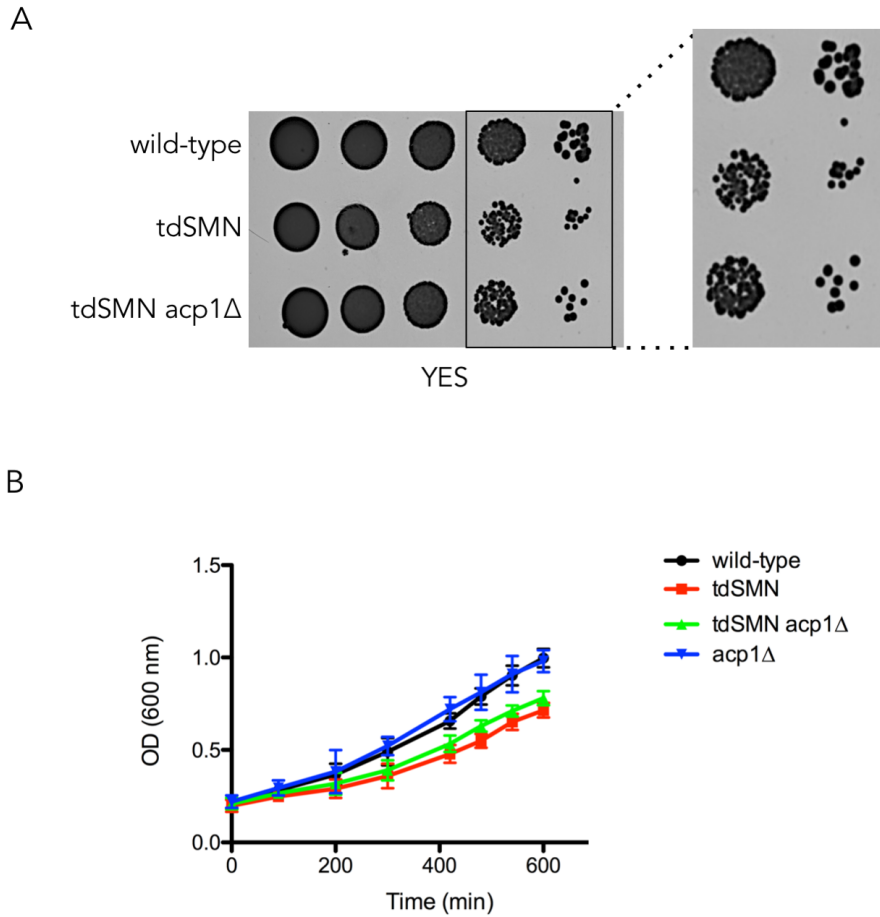
**Figure S1. Growth assays.** Related to Figure 1. A) The hypomorphic tdSMN mutant grows slower than wild-type and this phenotype can be suppressed by deletion of the non-essential *acp1*⁺ gene. Indicated cells were grown in YES media and serial dilutions were spotted on YES plates which were incubated at 25°C. The experiment was performed on three biological replicates. B) Growth curves of wild-type, *tdSMN*, *tdSMN acp1Δ* and *acp1Δ* cells. Exponentially growing cells were diluted in YES media and growth at 25°C was monitored. Error bars show means ± SD of three independent experiments.

**A**

| | Ladder | wild-type | tdSMN | tdSMN acp1Δ |

250
130
100
70
55
35
25
15
10
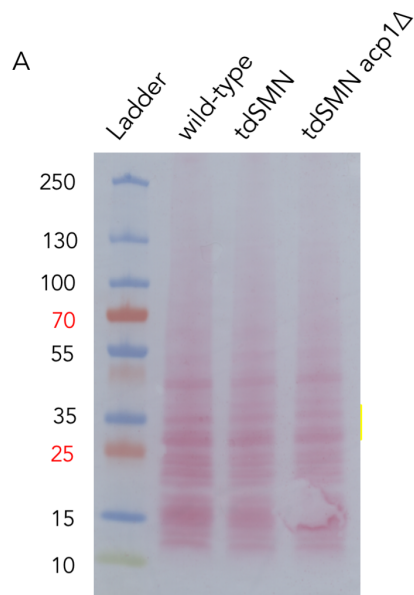
**B**

ImageJ quantification (A.U.)

| wt | tdSMN | tdSMN acp1Δ |
|---|---|---|
| 47951 | 37690 | 33527 |

**Figure S2. Characterization of F-actin levels in yeast strains.** Related to Figure 1A-B. Extracts of the indicated strains were prepared using the procedure described in the Cytoskeleton$^R$ F/G-actin assay kit and equal amounts were loaded on SDS-PAGE gels. After transfer to a nylon membrane, the blot was stained with Red Ponceau (A). Normalization of loading has been performed based on Ponceau-red staining and ImageJ quantification (B). The PageRuler$^{TM}$ Plus prestained protein ladder has been used and the apparent molecular weights (in kDa) of the protein bands are shown at left.
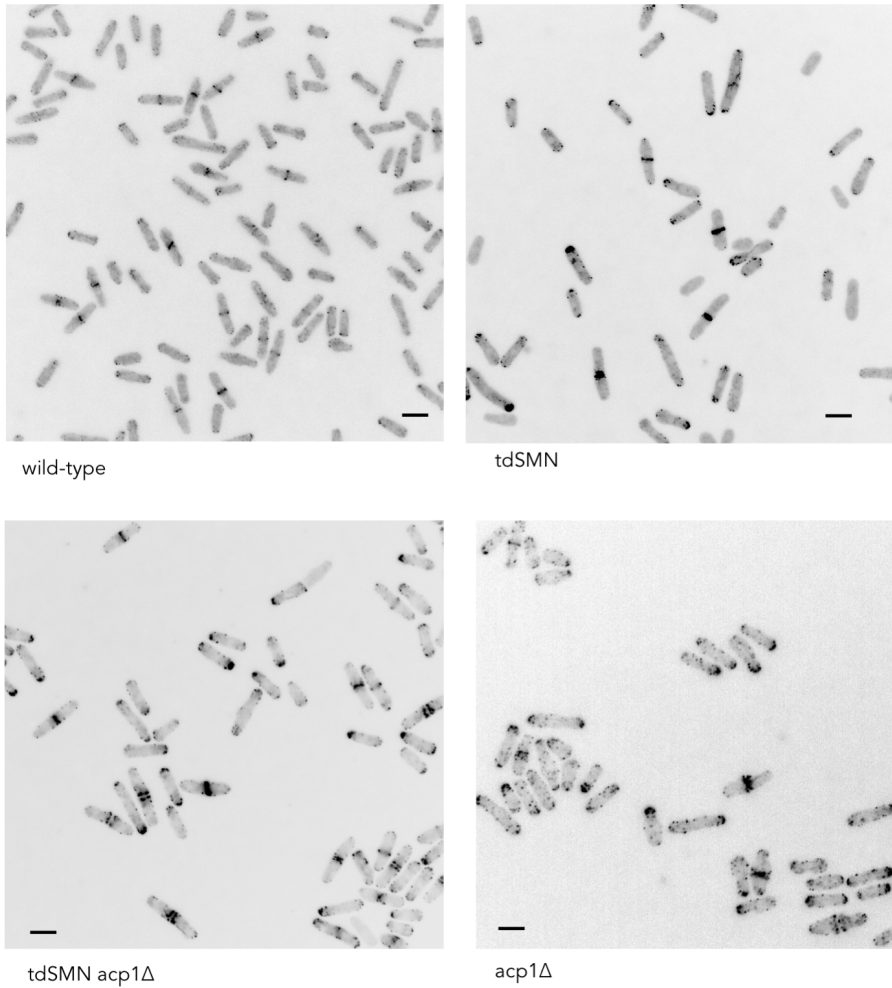
wild-type

tdSMN

tdSMN acp1Δ

acp1Δ

**Figure S3. Images of strains after Alexa Fluor® 488 Phalloidin staining.** Related to Figure 1C-D. Images of the indicated strains were captured using the Zeiss AxiolImager Z2 microscope and Methamorph software. The data shown are representative of three independent experiments. Scale bars, 4 μm.
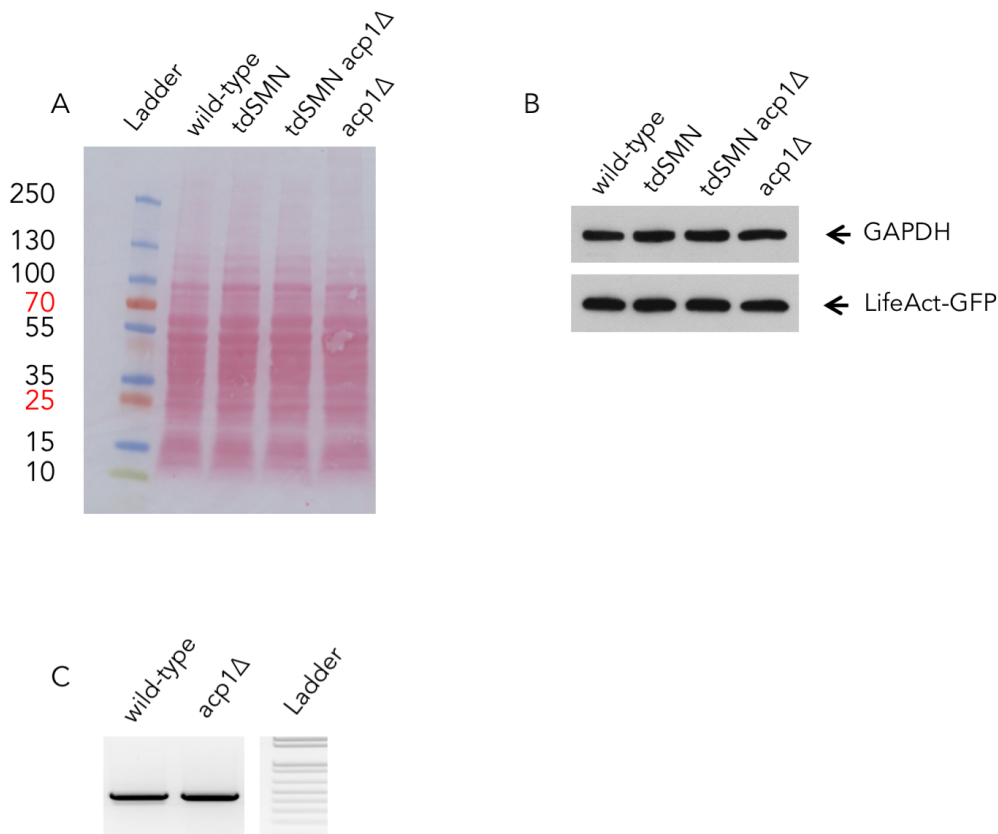
**Figure S4. Characterization of strains carrying an integrated LifeAct-GFP reporter.** Related to Figure 2.

A) Extract from yeast transformants were prepared and separated on SDS-PAGE. After transfer to a nylon membrane, the blot was stained with Red Ponceau. The PageRuler™ Plus prestained protein ladder has been used and the apparent molecular weights (in kDa) of the protein bands are shown at left. B) Characterization of strains expressing similar levels of LifeAct-GFP. The blot shown in panel A was blotted with anti-GFP and anti-GAPDH antibodies. After normalization to Red ponceau staining and GAPDH levels, quantification shows that the indicated strains express equivalent levels of LifeAct-GFP.

C) Splicing analysis. Related to Figure 3A. RT-PCR analyses were performed on total RNA isolated from the wild-type and *acp1Δ* cells grown at 25°C for introns located in the *S. pombe cdc3+* gene coding for profilin. The PCR products were separated on a 1.5% agarose gel and visualized by ethidium bromide staining. The marker corresponds to the Invitrogen 1Kb Plus DNA ladder.
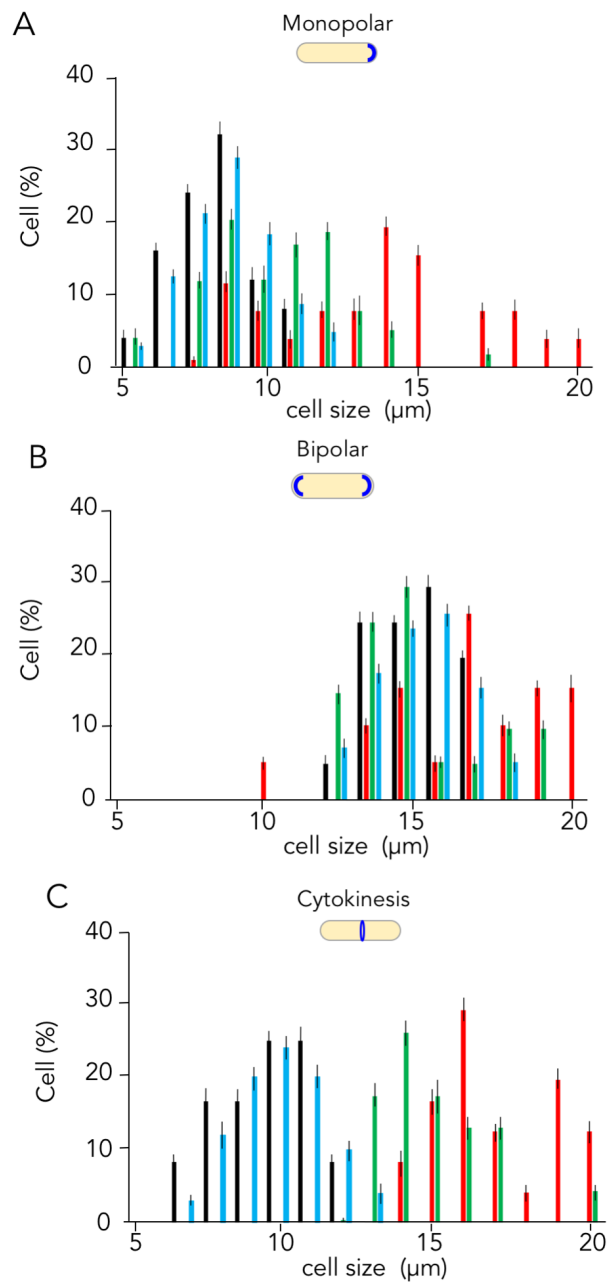
**Figure S5. Cytokinesis defect of *tdSMN* mutant cells.** Related to Figure 2C. Quantification of panels in Figure 2A showing percentage of cells with corresponding cell sizes (in μm) for cells having actin localized as monopolar, bipolar or at the cytokinetic ring. The data are similar to those shown in Figure 2C but are represented as histograms. Error bars show the SD of three independent experiments (n=100).
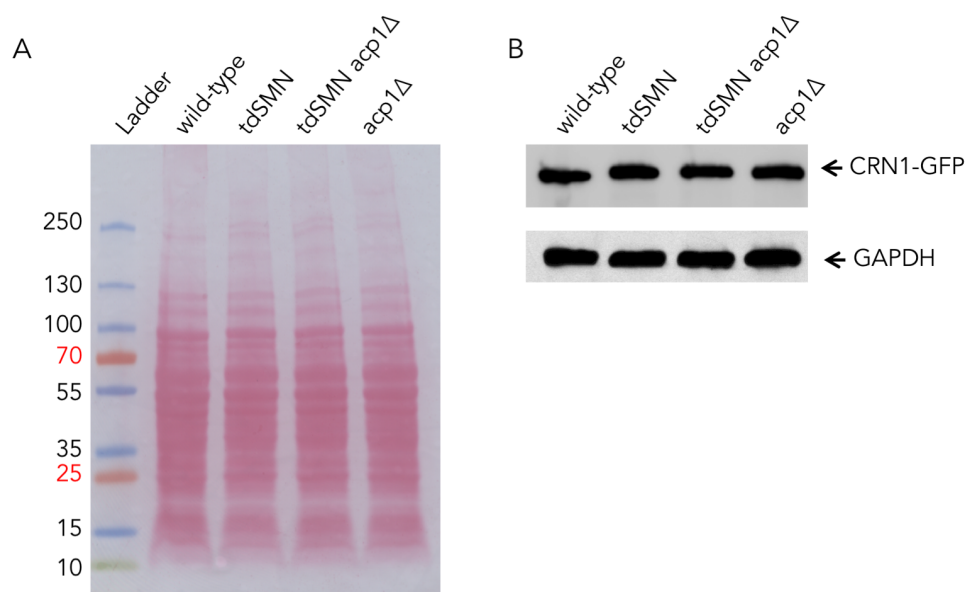
**Figure S6. Characterization of Crn1-GFP levels.** Related to Figure 3F.

The Crn1-GFP fusion protein is expressed at similar levels in wild-type, *tdSMN*, *tdSMN acp1Δ* and *acp1Δ* cells. Whole cell extracts were prepared from the indicated strains carrying an endogenous Crn1-GFP gene. After transfer to a nylon membrane, the blot was stained with Red Ponceau. The PageRuler™ Plus prestained protein ladder has been used and the apparent molecular weights (in kDa) of the protein bands are shown at left (A). Immunoblotting was performed with anti-GFP and anti-GAPDH antibodies (B). After normalization to Red ponceau staining and GAPDH levels, quantification shows that the indicated strains express equivalent levels of Crn1-GFP.
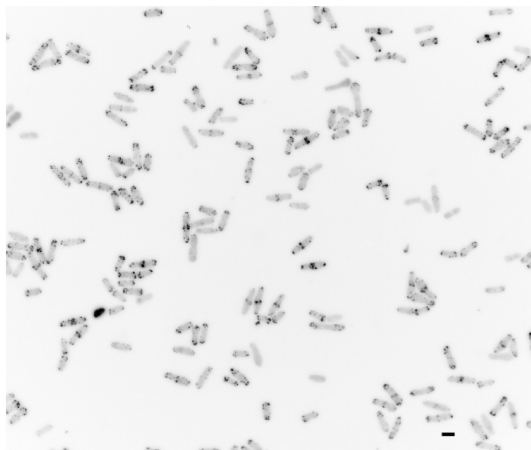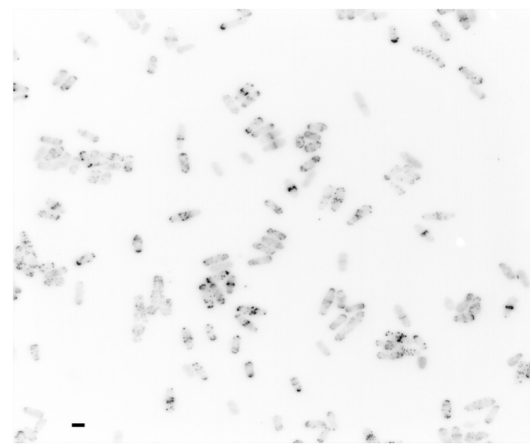
wild-type
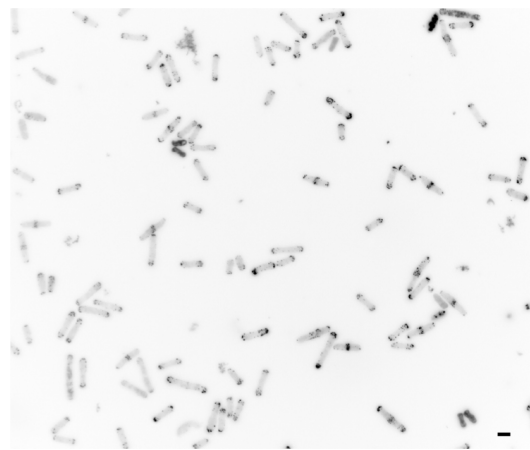
tdSMN
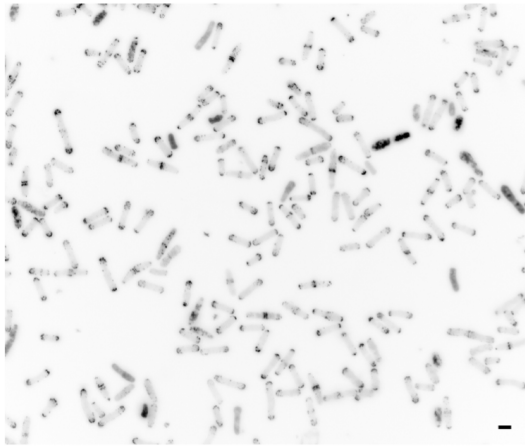
tdSMN acp1Δ

acp1Δ

**Figure S7. Images of strains carrying a Crn1-GFP reporter.** Related to Figure 3F. Images of wild-type, *tdSMN*, *tdSMN acp1Δ* and *acp1Δ* cells expressing a Crn1-GFP fusion protein, were captured using the Zeiss AxiolImager Z2 microscope. Scale bars, 4 μm.
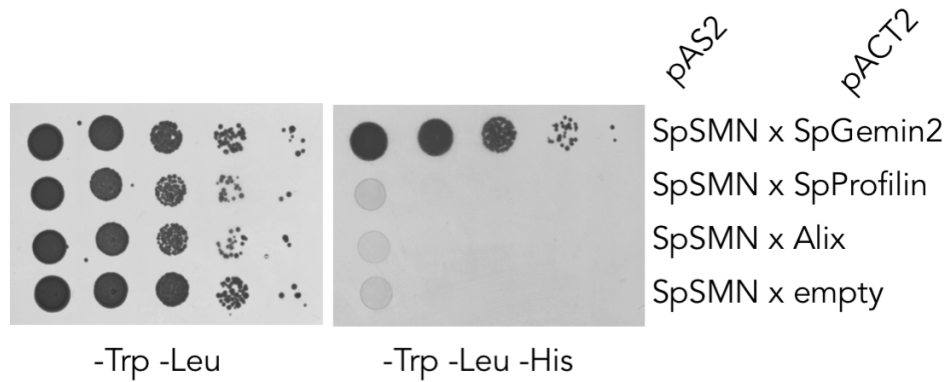
**Figure S8. Two-hybrid interaction assays.** Related to Figure 3A. The interaction between profilin and SMN from *S. pombe* was determined by the yeast two-hybrid system by measuring the activation of the HIS3 reporter gene (Durfee et al., 1993). pAS2 an pACT2 express the indicated genes fused to the Gal4 DNA binding domain and the Gal4 activation domain, respectively. The *S. pombe* Gemin2 is known to interact with SMN and has been used as positive control. An empty vector or the unrelated Alix protein served as negative controls. Three independent experiments were performed, and the result of one representative is shown.

## Transparent Methods

### Strains, culture conditions and genetic methods

Yeast strains used in this study are listed in Table S2. Standard methods were used for growth and genetic manipulation of *S. pombe* (Moreno *et al*, 1991). Cells were grown on YES or minimal EMM2 (USBiological, Cat# E2205) medium with adequate supplements. Latrunculin A was obtained from Sigma (Cat# L5163).

The *tdSMN* degron allele was constructed using the pSMRG2-nmt41-degronHA plasmid (Campion et al., 2010). A DNA fragment carrying 400 nucleotide homologies to genomic DNA was amplified and transformed into fission yeast PEM2 cells (Roguev et al., 2007). Correct homologous recombination of the tagged allele was checked by PCR.

The haploid strain carrying the null allele of *acp1/SPAC12B10.07* (*h+ ade6-M210 ura4-D18 leu1-32 SPAC12B10.07::KanMX4)* was obtained from Bioneer Corporation (Korea). The double mutant *tdSMN acp1Δ* strain was constructed by crossing *tdSMN* and *acp1Δ* haploids on Malt media. After sporulation, spores were dissected and germinated at 25°C on YES plates. Cells corresponding to the *tdSMN acp1Δ* double mutant were identified by replica plating to YES medium containing 100 µg/ml geneticin (G-418). Correct integrated and disrupted alleles were checked by PCR amplification of genomic DNA.

To construct strains carrying the LifeAct-GFP reporter, we used the integrative pJK148 plasmid (pJK148-P*act1*-LifeAct-GFP) (Huang et al., 2012), which was a kind gift from Dr. M. Balasubramanian. The plasmid was digested by NruI within the *leu1*$^+$ gene and transformed into wild-type, *tdSMN*, *tdSMN acp1Δ* and *acp1Δ* yeast cells. The transformants were selected on minimal medium lacking leucine and the colonies were further screened visually for fluorescence. Correct and similar expression of the LifeAct-GFP protein in the different strains was tested by Western blot analysis (Figure S4).

Strains carrying a C-terminal tagged CRN1-GFP allele were constructed by PCR-based one-step homologous recombination (Bähler et al., 1998). The integrating cassette was amplified by PCR from plasmid pYM25 (Euroscarf, Cat# P30236) (Janke et al., 2004), using 400 nucleotides flanking sequence homology on each side of the genomic insertion site. The bacterial strain Top10 (Thermofischer, Cat#C4040-50) was used to amplify plasmids. Correct and similar expression of the Crn1-GFP protein in the different strains was tested by Western blot analysis (Figure S6).

## Yeast two-hybrid analyses

Two-hybrid assays were performed with the CG1945 and Y187 strains, the baits and preys having been cloned into the pAS2 and pACT2 vectors, respectively (Fromont-Racine et al., 2002). Primer sequences and PCR regimes are available upon request. The CG1945 strain was transformed with the bait pAS2-SpSMN containing the gene sequence fused in frame with the GAL4 DNA-binding domain (GAL4-BD) and selected on –Trp plates. The Y187 strain was transformed with the pACT2 constructs containing the gene sequences fused in frame with the GAL4 activation domain (GAL4-AD) and selected on –Leu plates. Bait and prey strains were mated overnight on rich YPD plates and diploids containing bait/prey combinations were selected on –Trp–Leu plates. Diploid yeast cells carrying bait/prey combinations were cultured in –Trp–Leu media and interactions were screened by spotting serial dilutions on –Trp–Leu–His plates. Incubations were performed at 30°C for 3-5 days.

## F/G actin preparation

Extract were prepared using the F/G *in vivo* actin assay kit (Cat# BK037, Cytoskeleton, Inc, Denver, USA). Briefly, after centrifugation, pellets were washed with water and resuspended in Lysis and F-actin stabilization (LAS2) buffer (containing 1 mM ATP and protease inhibitor) to 0.2 g cells/ml. Cells homogenates were frozen in liquid nitrogen and ground to fine powder using a Freezer Mill 6770 grounder (Spex). The powder was then thawed and incubated for 10 min at 37°C, after homogenization of the lysate by passing through a 25G syringe. 1.5 ml of lysates was centrifuged at 6000 rpm (room temperature, 10 min) to pellet unbroken cells or cellular debris. The supernatant (1 ml) was recovered and spun at 55 000 rpm for 1 hour at 37°C in a TLA-100.3 rotor. The supernatant (G-actin fraction) was recovered and the pellet (F-actin fraction) was dissolved in 1 ml of F-actin depolymerization buffer and aliquots were stored at -80°C. SDS-PAGE separation, performed using TGX-precast gel (Cat# 4561083, BioRad), was followed by Western blot analysis using Nitrocellulose Protran BA85 (Whatman, Cat# 10401196) and ECL Western Blotting Detection Reagent (GE Healthcare, Cat# RPN 2106).

Total crude protein extracts were also prepared from five $OD_{600nm}$ units of yeast cells, by the NaOH-TCA lysis technique (Matsuo et al., 2006).

## Antibodies

The following antibodies have been used in this study : actin (Cytoskeleton kit, Cat# AAN01, RRID:AB_10708070), Actin (cloneC4, Millipore Cat#MAB1501, RRID :AB_2223041), GFP

(Chromotek Cat#3H9-20, RRID:AB_10773374), GAPDH (Abcam, Cat# Ab8245, RRID:AB_2107448), Profilin (S. pombe, kindly provided by V. Sirotkin), anti-rabbit secondary (Abcam, Cat# ab6721, RRID:AB_955447), anti-mouse secondary (Abcam, Cat# ab6728, RRID:AB_955440)

**RT-PCR analysis**

For RT-PCR analyses, total RNA was purified from exponentially growing cells with Tri-Reagent (Sigma, Cat# T9424) according to the manufacturer's procedure and treated with RQ1 RNase-free DNase (Promega, Cat# M6101). First strand cDNAs were synthesized from 5 μg of total RNA and pd(N)6 random oligonucleotides with First strand cDNA synthesis kit (GE Healthcare, Cat# 27926101). For PCR analyses, 1/10 of the reaction was amplified with GoTaq polymerase (Promega), and the cycle number was kept to a minimum to maintain linearity. Specific primers (IDT DNA) used in our work are described in Table S3. PCR regimes are available upon request. PCR products were separated on 1.5-2% agarose gels containing ethidium bromide and visualized under UV light.

**Cytology**

To monitor endocytosis in fission yeast, cells were labelled with the lipophilic dye FM4-64, according to the method described by Vida and Emr (1995). Cells were grown to an optical density (OD600) of 0.5, harvested by centrifugation and resuspended in 400 μl cold media containing FM4-64 (Life Technologies, Cat# T13320) at a final concentration of 8μM. Cells were then transferred to an imaging chamber and images were captured in a single focal plan and the light intensity recorded for 20 cells at each time point. Phalloidin staining was performed as described in Chang et al. (1996). Briefly, cells were grown in 5 ml YES and fixed by the addition of 5 ml formaldehyde-PM (40% of EM-grade methanol-free formaldehyde 16% and 60% PM (35 mM KPO$_4$, pH 6.8, 0,5 mM MgSO$_4$)) for 15 minutes. Cells were washed 3x with PM and permeabilized with PM+1% Triton X-100 for 2 minutes. Cells were washed 3x with PM and cell pellets were incubated in Alexa Fluor 488-phalloidin (Molecular Probes) for 30 minutes at room temperature. Cells were mounted in Vectashield mounting medium (Vector Laboratories) containing DAPI (4',6'-diamidino-2-phenylindole dihydrochloride).

**Image acquisition and analysis**

Images were acquired with a Zeiss AxiolImager Z2 microscope using the MetaMorph software (Roper Scientific, San Diego, CA). Fluorescence quantification was performed with ImageJ

(version 2.0.0) using an extension, kindly provided by Sylvain de Rossi (MRI, CNRS Montpellier), which was set to accept *S. pombe* cells with correct size and shape and used to calculate corrected total cell fluorescence (CTCF) (MacCloy et al., 2014). The data was collated in Microsoft Excel and analyzed for statistical significance in GraphPad Prism (v.5.00, GraphPad Software, USA) using two-way ANOVA with Tukey's multiple comparisons tests or 2-sided unpaired Student *t* tests.

**Supplemental References**

Bähler, J., Wu, J.Q., Longtine, M.S., Shah, N.G., McKenzie, A., Steever, A.B., Wach, A., Philippsen, P., Pringle, J.R. (1998). Heterologous modules for efficient and versatile PCR-based gene targeting in Schizosaccharomyces pombe. Yeast *14*, 943–951

Campion, Y., Neel, H., Gostan, T., Soret, J., Bordonné, R. (2010). Differential splicing defects in fission yeast cells carrying a temperature-degron allele of the Survival of Motor Neuron gene. EMBO J. *29*, 1817-1829

Chang, F., Woollard, A., Nurse, P. (1996). Isolation and characterization of fission yeast mutants defective in the assembly and placement of the contractile actin ring. J Cell Sci. 109, 131-42.

Durfee, T., Becherer, K., Chen, P.L., Yeh, S.H., Yang, Y., Kilburn, A.E., Lee, W.H., Elledge, S.J. (1993) The retinoblastoma protein associates with the protein phosphatase type 1 catalytic subunit. Genes Dev *7*, 555-569.

Fromont-Racine, M., Rain, J.C., Legrain, P. (2002). Building protein-protein networks by two-hybrid mating strategy. Methods Enzymol *350*, 513–524.

Huang, J., Huang, Y., Yu, H., Subramanian, D., Padmanabhan, A., Thadani, R., Tao, Y., Tang, X., Wedlich-Soldner, R., Balasubramanian, M.K. (2012). Nonmedially assembled F-actin cables incorporate into the actomyosin ring in fission yeast. J Cell Biol *199*, 831-847.

Janke, C., Magiera, M.M., Rathfelder, N., Taxis, C., Reber, S., Maekawa, H., Moreno-Borchart, A., Doenges, G., Schwob, E., Schiebel, E., Knop, M. (2004). A versatile toolbox for PCR-based tagging of yeast genes: new fluorescent proteins, more markers and promoter substitution cassettes. Yeast *21*, 947-62.

Matsuo, Y., Asakawa, K., Toda, T., Katayama, S. (2006). A rapid method for protein extraction from fission yeast. Biosci. Biotehnol. Biochem. *70*, 1992-1994.

McCloy, R.A., Rogers, S., Caldon, C.E., Lorca, T., Castro, A., Burgess, A. (2014). Partial inhibition of Cdk1 in G 2 phase overrides the SAC and decouples mitotic events. Cell Cycle 13,1400-1412.

Moreno, S., Klar, A., Nurse, P. (1991). Molecular genetic analysis of the fission yeast Schizosaccharomyces pombe. Methods Enzymol *194*, 795–823

Roguev, A., Wiren, M., Weissman, J.S., Krogan, N.J. (2007). High-throughput genetic interaction mapping in the fission yeast Schizosaccharomyces pombe. Nat. Methods *4*, 861-866

Vida, T.A., Emr, S.D. (1995). A new vital stain for visualizing vacuolar membrane dynamics and endocytosis in yeast. J Cell Biol *128*, 779-792.